Analyst

Accepted Manuscript

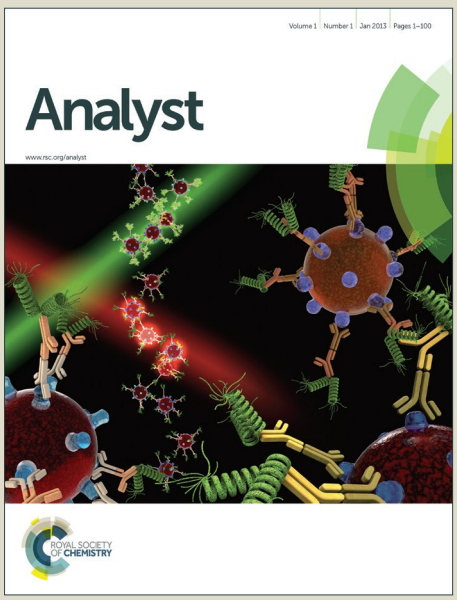

ROYAL SOCIETY OF CHEMISTRY

www.rsc.org/analyst

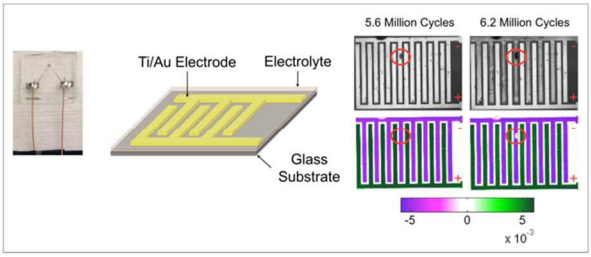

The electroreflectance technique is shown to be an effective method for visualizing ageing behavior of microsupercapacitors.

Journal Name

ARTICLE TYPE

Cite this: DOI: 10.1039/xxxxxxxxxx

Electroreflectance imaging of gold-H_3PO_4 supercapacitors. Part II: Microsupercapacitor ageing characterization†

Kimberly R. Saviers,[a] Arpan Kundu,[a] Kerry Maize,[b] Ali Shakouri,[b] and Timothy S. Fisher[a‡]

Received Date
Accepted Date

DOI: 10.1039/xxxxxxxxxx

www.rsc.org/journalname

This microsupercapacitor ageing study demonstrates the usefulness of the electroreflectance technique by quantifying local charge accumulation. Two separate devices with interdigitated electrodes were evaulated over a period of 4.1 million charge/discharge cycles. The key results are spatial mapping of charge accumulation in the gold electrodes derived from variation in the observed electrode reflectance. The nominal device exhibited little change in spatial distribution throughout the ageing cycle and serves as a comparison for the test device, which exhibited some nonuniform charge accumulation behavior. Further, an accelerated ageing test was completed by applying increasing voltage pulses up to 1.46V to the device. Visual evidence of electrode ageing emerged in the reflectance distribution. An equivalent circuit model was developed to assess the evolution of individual circuit elements that correlate to the physical causes of ageing.

1 Introduction

As portable electronics decrease in size, conventional energy storage components such as batteries, fuel cells, and capacitors become less suitable due to their size and weight. Modern microfabrication technology has led to miniaturized energy storage devices such as microbatteries[1] and microsupercapacitors[2] that can be integrated with electronic devices. Microsupercapacitors offer advantages over their battery counterparts in terms of high rate capability and long cyclic stability. They store charge through reversible ion adsorption at the electrode/electrolyte interface, allowing charge/discharge at very high rates. However, their energy density is lower than that of batteries.[2]

Most of the notable advancements in the microsupercapacitor field in the past decade have involved improvements in energy density with nanostructured electrode materials[3,4,5,6,7] as well as unique fabrication methods[8] featuring flexible substrates[9,10,11]. Comparatively less focus has been given to evaluating cyclic stability and operation lifetime. Lifetime prediction and the evaluation of degradation behavior of such devices is critical to the reliability of the entire system including the electronic devices that they power.

Supercapacitor ageing is caused by degradation of the electrode materials and the electrolyte and is sensitive to different types of device usage. Mechanisms include a decrease in active electrode surface area, decrease in electrolyte conductivity, and the presence of parastic electrochemical reactions. In one particular study, El Brouji et al.[12] showed that blockage of electrode pores occurred only in ageing by charge cycling, resulting in greater capacitance loss, as opposed to electrically floating the device for up to 4000 hours. Device temperature can also be a contributing factor to ageing, as demonstrated by Bohlen et al.[13] in an impedance model showing that temperature and voltage create a self-accelerating feedback cycle with ageing of the device. In microsupercapacitors, voltage is a greater concern than internal heat generation due to low operating currents; however, thermal characterization of microsupercapacitors remains largely unstudied[14].

Further, some prior studies have reported initial increases in capacitance upon prolonged use. Ratajczak et al.[15] reported an initial increase in capacitance when electrically floating activated-carbon capacitors in aqueous Li_2SO_4 electrolyte. The effect appeared to be stronger at elevated temperatures and was attributed to better wetting of the electrode material by the electrolyte. Lu et al.[16] studied capacitor with TiN electrodes and KOH electrolyte with a cyclic capacitance that increased by 20% near the $1{,}000^{th}$ cycle followed by an immedate drop below 10% relative to the initial capacitance. El Brouji et al.[12] observed capacitance recovery in rest periods between cycling tests and attributed the result to impurities moving away from pores.

Other studies have shown that positive and negative electrodes behave differently in response to ageing. In an accelerated ageing

Birck Nanotechnology Center, Purdue University, West Lafayette, IN, USA
[a] *School of Mechanical Engineering*
[b] *School of Electrical and Computer Engineering*
‡ *E-mail: tsfisher@purdue.edu*

study of activated-carbon supercapacitors with Et_4NBF_4 in acetonitrile electrolyte, Cericola et al.[17] showed that the negative electrode gradually increased in capacitance while the positive electrode exponentially decreased in capacitance. This behavior changed significantly for different electrolyte compositions and electrode mass ratios. Lastly, in a detailed study utilizing XPS, Raman and IR spectroscopies, and posimtery, Bettner et al.[18] found that the negative electrode suffered more in the case of carbon-based electrode materials.

An ageing study with the electroreflectance measurement technique enables observation of non-idealities, how they evolve over time, and their effects on device capacitance. Visualization of a spatial map of charge accumulation in supercapacitor electrodes can be achieved by measuring the change in reflectance of the device resulting from an input electrical signal. The measurement enhances more conventional measurement techniques such as cyclic voltammetry (CV) and electrochemical impedance spectroscopy (EIS), which are used to study average device performance characteristics. The reflectance change observed in an experiment can be attributed to electric field modulation of the optical properties of gold, as concluded on the basis of a series of studies completed in the 1960s and 1970s[19,20,21,22,23,24]. Electroreflectance is a change in the refractive index of the electrode caused by charge formation. Hence, free electron theory was chosen here for the electroreflectance model to calculate the reflectance change of the gold microsupercapacitor.

The study herein includes experimental and subsequent model analysis of a microsupercapacitor. Both a nominal device and a device exhibiting "burn-in" behavior were studied for mutual comparison. A total of 4.1 million cycles were applied to each device at a high charge/discharge rate while the capacitance and electroreflectance signals were periodically recorded. Next, an additional 2.0 million cycles were applied to the nominal device at increased voltages in order to accelerate ageing. Electroreflectance was utilized to obtain information about the degradation occurring in the device with repeated cycling. Lastly, both an equivalent circuit model and electroreflectance model were employed to bring further insight into the cause of ageing.

2 Experimental Methods

2.1 Sample Fabrication

Interdigitated microsupercapacitor electrodes were fabricated by electron-beam deposition of Ti (10 nm) and Au (80 nm) on a glass slide followed by conventional photolithography and wet chemical etching. Each electrode consisted of eight electrode fingers measuring 40 μm wide and 600 μm long with spacing 20 μm between opposite electrodes.

The electrolyte was composed of H_3PO_4 suspended in a polyvinyl alcohol (PVA) polymer matrix. It was prepared by combining ultra-pure water, concentrated phosphoric acid, and powdered PVA (molecular weight 89,000-98,000, 99+% hydrolyzed, Sigma-Aldrich) in a 1:1:10 ratio by weight and vigorously mixing at 90°C until clear. Using a micropipette, 10 μL of electrolyte solution was applied to the microsupercapacitor electrodes and cured for several days in ambient conditions. Cu wires were attached to electrode contact pads with solder.

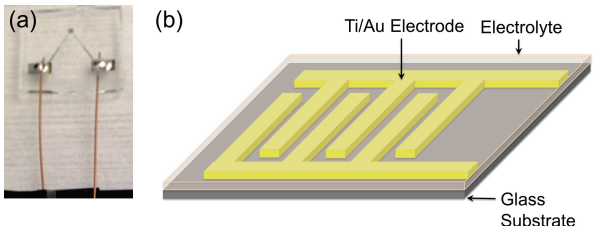

Fig. 1 (a) Photograph and (b) schematic of the microsupercapacitor device. The device consisted of eight interdigitated fingers on each electrode; three fingers are shown here as an example.

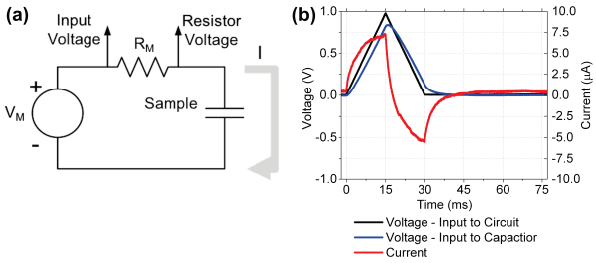

Fig. 2 (a) Diagram of the circuit configuration used in the electroreflectance experiments where R_M = 22 kΩ. (b) Example of the voltage and current signals measured in the electroreflectance experiments. The full cycle length was 150 ms. Data shown is the signature at 1.5 million cycles of the microsupercapacitor with burn-in behavior, which is the maximum signal observed.

A schematic and photograph is displayed in Fig. 1. The device stores charge by forming an electrostatic double layer at each electrode-electrolyte interface and is thus termed a supercapacitor. In contrast, an electrolytic capacitor stores electrostatic charge across a dielectric layer, often composed of an oxide material.[25] In the microsupercapacitor, the phosphoric acid electrolyte dissocates primarily into H^+ and $H_2PO_4^-$ ions. Upon charging, these ions are respectively attracted to the negative and positive electrodes.

An electroreflectance method was used to study the distribution of charge in the microsupercapacitor electrodes. The method is described in detail in the companion paper by Maize et al.[26] The optical reflectance of the electrodes changes due to the accumulation of electrons in the conduction band, thus resulting in a spatial distribution image of the microsupercapacitor. This measurement was performed with two separate devices: one defect-free and the other showing charactistics of a decreased initial capacitance. Next, high voltages were applied to the defect-free sample to induce accelerated ageing.

2.2 Sample Measurement

A RC circuit enabled extraction of the microsupercapacitor charge and discharge current, as shown in Fig. 2 where R_M = 22 kΩ. A triangular voltage pulse at 20% duty cycle was repeatedly applied to the circuit in three intervals corresponding to charge, dis-

charge, and rest as given in volts by

$$v_M(t) = \begin{cases} 66.67 * t, & 0.000 < t < 0.015s \\ 2 - 66.67 * t, & 0.015 < t < 0.030s \\ 0, & 0.030 < t < 0.150s \end{cases} \quad (1)$$

An example of the voltage and current signals is shown in Fig. 2. For ideal capacitor behavior, the current shape would be a step function. Simultaneously, a pulsed light ($\lambda = 530$ nm) illuminated the sample while the reflectance signal was recorded through a 10x lens. Each image respresents the normalized difference in reflectance between two images: one recorded just before the voltage is applied and one recorded at varying times during the voltage cycle.

The microsupercapacitor was cycled for a period of eight days, with the exception of routine de-mounting of the device for cyclic voltammetry (CV) measurements. The CV curves were measured using a BASi Epsilon electrochemical system at 13 different scan rates ranging from 25 mV/s to 25,000 mV/s. The number of cycles performed with the device was calculated based on the elapsed cycling time and cycle period length (150 ms) with the electroreflectance system plus the number of cycles performed for the CV measurements. The device remained in laboratory ambient conditions for the duration of the study (19.0 - 21.5°C; 35 - 50% relative humidity).

2.3 Experimental Analysis Method

An image processing scheme was developed in MATLAB in order to extract the mean, standard deviation, skewness, kurtosis, and probability distribution (histogram) from the electrode area in each reflectance image. Only the mean and standard deviation are presented here for clarity. The program generated a mask from each high-contrast CCD image that was then utilized to extract the reflectance intensity associated with each electrode from the reflectance image. Conceptually, the data not only provide insight into the magnitude of reflectance change and the distribution of the intensity across each electrode, but also how these two characteristics changed during each voltage cycle and throughout the entire ageing study.

3 Model Formulation

An equivalent circuit model enables further understanding of the physical phenomenoa occurring in the device, while an electroreflectance model verifies the experimental reflectance results. An abbreviated description of both an electroreflectance and circuit model is included here, while the companion paper[26] provides a full presentation of each model.

3.1 Equivalent Circuit Model

The circuit model was fit to the measured current to extract individual equivalent circuit elements and to quantify the accumulated charge. Because the device was expected to behave as a pure electrical double layer capacitor, it was modeled as a Randles circuit[27] consisting of an equivalent series resistance (ESR) R_s in series with a parallel combination of double layer capacitor C_{dl} and leakage resistance R_L as shown in Fig. 3. In general, factors contributing to ESR in a supercapacitor include (i) electrolyte resistance, (ii) contact resistance between the electrode and current collector, (iii) bulk resistance of the electrode material, and (iv) resistance of ions migrating through the separator.[28]

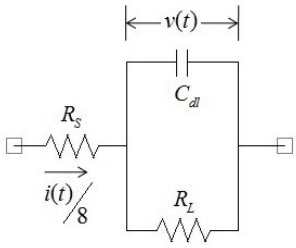

Fig. 3 Randles equivalent circuit for a single electrode finger. The full device was modeled by considering eight of these circuits in parallel and assuming that each finger is identical.

The leakage resistance R_L represents the phenomenon of self-discharge during which the device spontaneously loses charge. It causes the input current during charge to be greater than the output current during discharge. Physical mechanisms of self-discharge include ohmic leakage, parasitic Faradaic reactions, and charge redistribution.[29] However, in this study charge redistribution can be considered insignificant due to the absence pores in the electrode material.[29]

Each finger pair of the present device represents a capacitor. N fingers of each polarity, in parallel, correspond to N capacitors in parallel. Thus the device consisting of 8 interdigitated fingers was represented by 8 equivalent parallel branches of Randles circuits. Based on the equivalent circuit, the expression governing the voltage $v(t)$ across C_{dl} is given by the following expression where $v_M(t)$ is defined in Eq. 1:

$$v_M(t) = (8R_M + R_s)C_{dl}\frac{dv(t)}{dt} + \frac{(8R_M + R_s + R_L)}{R_L}v(t) \quad (2)$$

The current $i(t)$ flowing through the main circuit can be calcuated as follows. One-eighth of $i(t)$ flows through each branch.

$$i(t) = 8(C_{dl}\frac{dv(t)}{dt} + \frac{v(t)}{R_L}) \quad (3)$$

The current charging a single finger electrode $i_1(t)$ is given by

$$i_1(t) = C_{dl}\frac{dv(t)}{dt} = \frac{i(t)}{8} - \frac{v(t)}{R_L} \quad (4)$$

The total charge q accumulated in a single gold finger electrode is found by integrating $i_1(t)$. The unknown parameters of the model (R_s, C_{dl}, and R_L) were evaluated by matching the current $i(t)$ to the experimentally-measured current. The current profile was evaluated by considering all combinations of the parameters between the defined lower and upper limits and minimizing the mean square error, MSE_{curr}.

3.2 Electroreflectance Model

The electroreflectance model relates the electrode charge accumulation, as obtained previously, to the reflectance change. The

complex refractive index of gold is a function of its complex dielectric constant $\tilde{\varepsilon}$ defined as[30]

$$\tilde{n} = \sqrt{\tilde{\varepsilon}} \tag{5}$$

The dielectric constant consists of contributions from free electrons and bound electrons; however only free electrons contribute significantly[21] as follows

$$\tilde{\varepsilon}_f(\omega) = 1 - \frac{\omega_p^2}{\omega^2 + i\omega/\tau} \tag{6}$$

where τ is the frequency-dependent relaxation time of electrons in the conduction band[21,31], and ω is the incident light angular frequency. ω_p is the plasma frequency given by[32]

$$\omega_p = \sqrt{\frac{\eta e^2}{\varepsilon_0 m^*}} \tag{7}$$

where η is the free electron number density, e is the electron charge, m^* is the electron effective mass, and ε_0 is the permittivity of free space. A change in the free electron concentration $\Delta\eta$ induces a change in plasma frequency $\Delta\omega_p$ in a relation given by

$$\frac{\Delta\omega_p}{\omega_p} = (1 + \frac{\Delta\eta}{\eta_0})^{1/2} - 1 \tag{8}$$

where η_0 is the intrinsic electron concentration in gold ($5.9 \times 10^{28}/m^3$).

The refractive index values were considered to be shifted on the frequency axis by the same fraction that ω_p is shifted, at a fixed value of ω_p.[21] The excess electron number density ($\Delta\eta$) accumulating on the electrode surface is given by

$$\Delta\eta = \frac{q}{Aed} \tag{9}$$

where A is the surface area of a single finger electrode. d is the unknown skin layer thickness, which refers to the thickness of the gold layer participating in charge accumulation. A is estimated to be 43,275 μm^2, corresponding to $1/8^{th}$ of the total electrode area that is covered by the electrolyte.

The Fresnel laws of reflection were used to evaluate the differential reflectance $\frac{\Delta R}{R}$ for the three-medium model consisting of air ($\tilde{n}_1$ =1), an ion double layer whose thickness was assumed to be 100 Å ($\tilde{n}_2$=1.333)[19,20], and gold ($\tilde{n}_3$=0.818+2.285i in the uncharged state, $\lambda = 530nm$). The reflectance as a function of the reflection coefficient is given by

$$R = r_{123}^2 = \left\{ \frac{r_{12} + r_{23}e^{-2i\beta}}{1 + r_{12}r_{23}e^{-2i\beta}} \right\}^2 \tag{10}$$

where r_{123} is a reflectance coefficient[24,30], r_{ij} are reflectance coefficients from medium i to medium j, and β is the phase factor $\beta = \frac{2\pi\tilde{n}_2 t}{\lambda}$. Finally, the differential reflectance change was calculated at every time step from the expression

$$(\frac{\Delta R}{R})_{model} = \frac{R_{charged} - R_{uncharged}}{R_{uncharged}} \tag{11}$$

where $R_{uncharged}$ and $R_{charged}$ refer to the reflectance of the electrode in the nominal and charged states respectively.

In summary, the state of charge of the device dictates the free electron concentration, which affects the plasma frequency. The plasma frequency is related to the complex dielectric constant, which affects refractive index of the electrode and thus the reflectance property. Therefore, the variation of the state of charge upon charge or discharge of the device induced the electrode reflectance change.

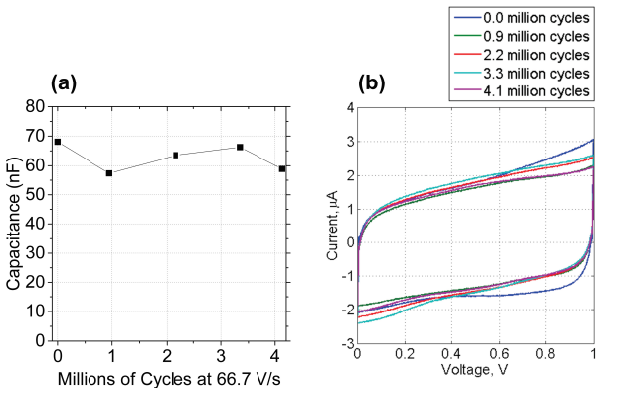

Fig. 4 (a) Measured capacitance and (b) CV curves at a scan rate of 25 V/s for the nominal microsupercapacitor.

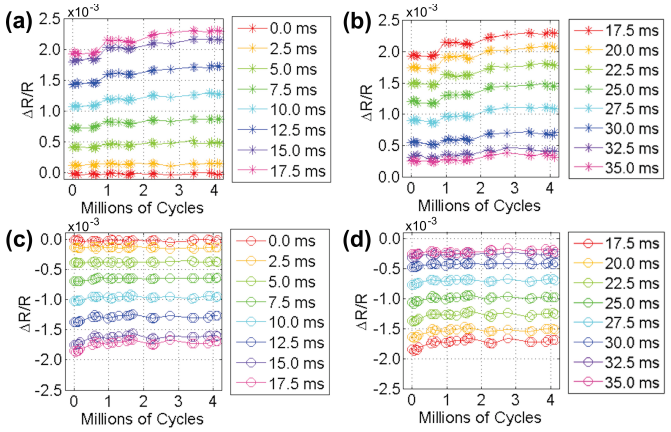

Fig. 5 Mean reflectance change for positive (star) and negative (circle) electrodes during charge (left) and discharge (right) phases for the nominal microsupercapacitor. (a) Positive electrode during charge phase, (b) positive electrode during discharge phase, (c) negative electrode during charge phase, and (d) negative electrode during discharge phase. Each data point was averaged over 2,000 cycles.

4 Results: Nominal Microsupercapacitor

The ageing experiment was first performed with a "nominal" microsupercapacitor with close-to-ideal behavior as a control for further samples. CV curves and capacitance values are shown in Fig. 4. The maximum scan rate of the capacitance measurements was 25 V/s, whereas the electroreflectance cycling scan rate was 66.7 V/s. These two scan rates were chosen to be as close as possible within the constraints of the measurement systems. There are no pseudocapacitance reactions present, and the microsupercapacitor is close to ideal. The capacitance remains at a fairly constant value throughout the cycling period, indicating that no significant

changes occurred to degrade the device performance at these cycling conditions.

This device was tested with the previously described electroreflectance technique. The reflectance change associated with the nominal microsupercapacitor is shown in Fig. 5. The magnitude of reflectance change was relatively constant throughout the testing period, as expected given the constant trend of capacitance. The positive electrode exhibited a slight increasing trend, which is considered small in this case. Reflectance images throughout the study indicated that charge accumulated uniformly on both electrodes during charge/discharge processes.

The time-series of reflectance change during each individual voltage pulse were very consistent in shape throughout the ageing period (not shown here for brevity; see Fig. 11 for an example). The shape of each series closely followed that of the voltage pulse applied to the device, while the reflectance change was positive on the positive electrode and was negative on the ground electrode. However, in general, the positive electrode reflectance change was slightly larger in magnitude than that of the negative reflectance change.

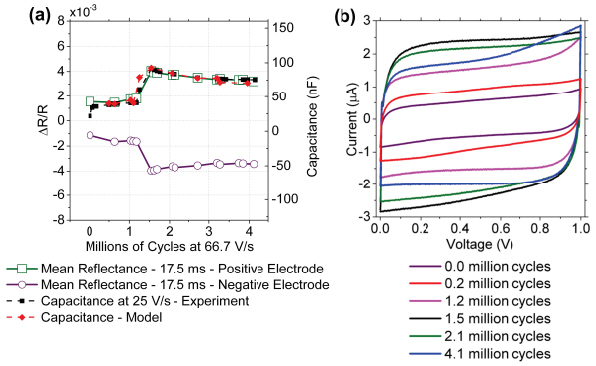

Fig. 6 (a) Mean reflectance change of each electrode at 17.5 ms into the voltage pulse and capacitance calculated from the equivalent circuit model. The corresponding capacitance at 25 V/s is shown for comparison, measured separately with CV curves shown in (b). Data corresponds to the microsupercapacitor with burn-in behavior.

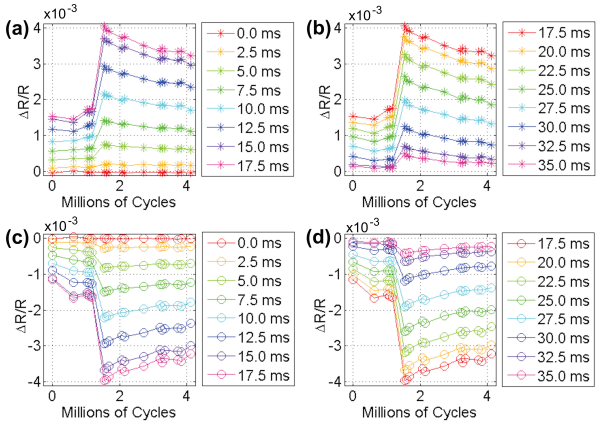

Fig. 7 Mean reflectance change for positive (star) and negative (circle) electrodes during charge (left) and discharge (right) phases for the microsupercapacitor with burn-in behavior. The graphs correspond to the (a) positive electrode during charge phase, (b) positive electrode during discharge phase, (c) negative electrode during charge phase, and (d) negative electrode during discharge phase. Each data point is averaged over 2,000 cycles.

5 Results: Microsupercapacitor with Burn-In Behavior

5.1 Experimental Results

A repeat measurement was performed on a sample exhibiting non-uniform charge accumulation on the negative electrode. Microsupercapacitor CV curves at various cycling times, capacitance values, and the mean reflectance of each electrode are displayed in Fig. 6. The CV curves were again relatively rectangular in shape, which is indicative of ideal electrochemical behavior.

A summary of the mean reflectance throughout the study is shown in Fig. 7. It is clear that a discontinuity in measured capacitance occurred between 1.2 and 1.5 million cycles. The CV curve shape indicates the device behaved more ideally at and beyond 1.5 million cycles. While no known external factor occurred to cause the sudden increase in capacitance, it provided an interesting feature to study the corresponding charge distribution. The relation between capacitance and reflectance along with several reflectance series associated with this device are presented in the electroreflectance modeling section below (Fig. 11).

Reflectance images before and after the sudden increase in capacitance are shown in Fig. 8 during charging, maximum charge, and discharging phases of operation. At 1.2 million cycles, an area on the negative electrode exhibited less charge accumulation than its complement area. The unactivated area became pro-

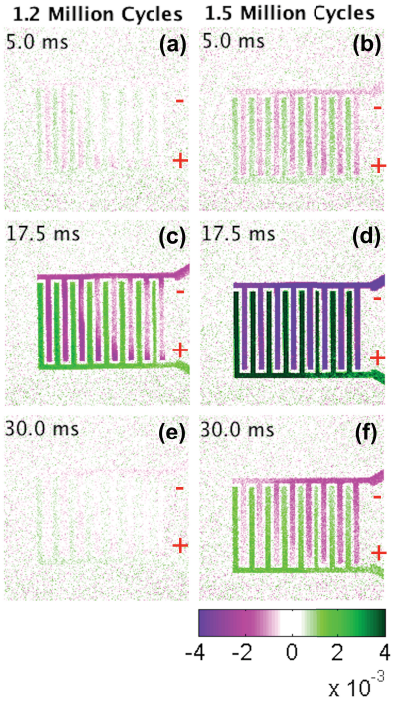

Fig. 8 For the microsupercapacitor with burn-in behavior, electroreflectance images before ((a,c,e)) and after ((b,d,f)) the discontinuous capacitance increase at time steps during charging (5.0 ms), charged (17.5 ms), and discharging (30.0 ms).

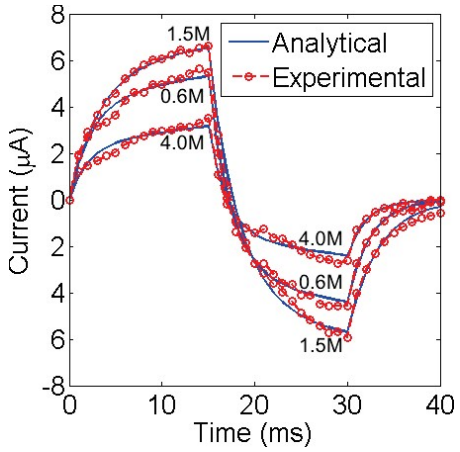

Fig. 9 Current and voltage profiles for various ageing conditions for the microsupercapacitor with burn-in behavior. Reported for various ageing conditions in millions of cycles.

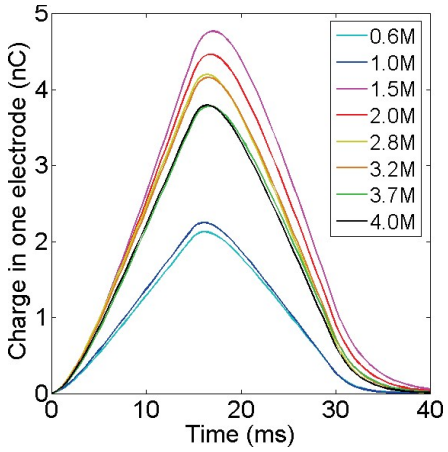

Fig. 10 Calculated charge accumulation in one positively charged finger electrode for the microsupercapacitor with burn-in behavior. Reported for various ageing conditions in millions of cycles.

gressively smaller from 0.0 to 1.2 million cycles until a sudden activation occurred. Therefore, at 1.5 million cycles, the area appeared to be fully activated.

Between 1.5 and 4.1 million cycles, the reflectance of each electrode decreased uniformly. These two distinct phases of ageing behavior suggested a change in dominance of two underlying physical mechanisms. We hypothesize that the first phase was dominated by decreased wetting of the electrolyte to the electrode, and the second phase was dominated by breakdown of the electrolyte. This point is supported further by the equivalent circuit model results presented below.

During the discharge phase when the electrodes were fully activated, as shown in Fig. 8(f), the charge dissipated away first from the area furthest from the electrode lead (bottom-left on the negative electrode). This effect was consistently observed throughout every discharge cycle recorded, and visually represents electrons funnelling out of the negative electrode during diffusive-dominated discharge. This pattern may be more subtle during the charging phase as the dominating mechanism is electrostatic force, which is likely to cause uniform charge accumulation.

5.2 Model Results

The microsupercapacitor with burn-in behavior was chosen for model analysis in order to understand its discontinuous behavior. The experimental and fitted model current profiles for various ageing conditions are shown in Fig. 9. For the experimenally-measured current profiles, the magnitude of the maximum current was larger than the magnitude of the minumum current. For example, for the ageing condition of 1.5 million cycles, the maximum was 6.7 μA while the magnitude of the minumum was 5.9 μA. This difference occurs because a fraction of the accumulated charge was dissipated by self-discharge.

The fitted circuit parameters of the electrical model are represented in Table 1 for various cycling conditions. The capacitance of the model device was obtained by multiplying C_{dl} by 8, because there were 8 electrode fingers each with capacitance C_{dl} in parallel. The device capacitance is compared with the experimentally-measured capacitance from CV measurements in Fig. 6.

Table 1 Fitted parameters for the microsupercapacitor with burn-in behavior. C_{dl} refers to the capacitance of a single finger electrode.

Millions of Cycles	C_{dl} (nF)	R_s (kΩ)	R_L (kΩ)	MSE_{curr}
0.6	4.9	250	9.5×10^{3}	4.1×10^{-14}
1.1	5.1	206	9.5×10^{3}	4.4×10^{-14}
1.5	12	119	1.1×10^{4}	5.8×10^{-14}
2.0	11	108	9.0×10^{3}	5.0×10^{-14}
2.8	9.8	75.4	7.5×10^{3}	5.0×10^{-14}
3.2	9.8	97.2	8.5×10^{3}	2.9×10^{-14}
3.7	9.0	141	8.0×10^{3}	3.4×10^{-14}
4.0	8.9	108	8.0×10^{3}	4.3×10^{-14}

We hypothesize that two different phenomenoa dominate the device performance at two different ageing phases. From 0.0 to 1.5 million cycles, the device increased in capacitance. Similarly, R_L increased and reached its highest value at 1.5 million cycles. In a comparable inverse trend, R_s experienced a significant decrease during this period. In other words, both values moved closer toward an ideal double layer capacitor ($R_L = \infty$ and $R_s = 0$). The trend in ESR supports the previously stated hypothesis that the initial capacitance trend occurs due to poor inital wetting of the electrolyte to the electrode, as also evidenced by the nonuniformity in the reflectance images (Fig. 8). By definition, as the electrolyte wets the electrode more effectively, ESR decreases.

In the second phase, from 1.5 to 4.1 million cycles, the device gradually decreased in capacitance. In this phase, the ESR fluctated and no significant degradation of the electrode was visible in the reflectance images. However, R_L gradually declined during this phase, and therefore was the dominant cause of ageing. This is likely to be a result from increasing ohmic leakage through conduction paths between the electrodes.

The fitted circuit parameters were used to quantify the charge accumulation in a single finger electrode capacitor C_{dl}, resulting in the values shown in Fig. 10. The external resistor in the measurement circuit induced an RC time constant, therefore causing the charge to reach maximum after the peak voltage (15 ms) and to reach zero after the end of discharge (30 ms). Throughout

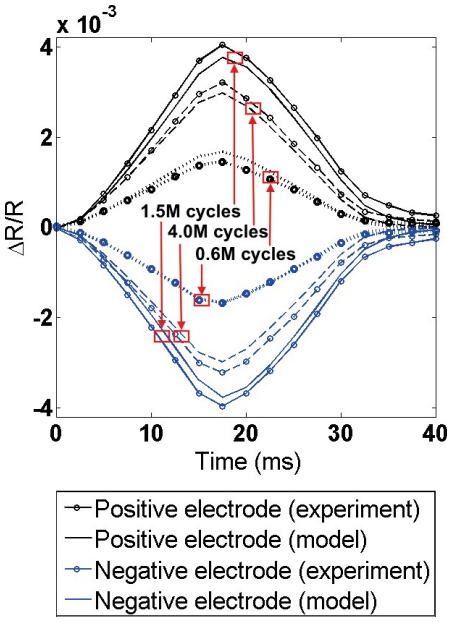

Fig. 11 Reflectance change obtained from model and experiment for various cycling conditions of the device with burn-in behavior.

ageing, the peak charge increased from its lowest value of 2.1 nC (0.6 million cycles) to a value of 4.7 nC (1.5 million cycles) and thereafter reduced to 3.8 nC (4.0 million cycles). As expected, this trend follows the trend of capacitance C_{dl} with ageing.

The reflectance change obtained from the model and the experiment are plotted in Fig. 11. The shape of the reflectance change with time followed closely that of the calculated charge variation with time. Also, the magnitudes of the positive and negative experimentally-observed reflectance change were approximately equal, agreeing well with the assumption that charge formation only perturbs the refractive index of gold. Overall, the reflectance change varies linearly with charge accumulation and thus capacitance.[26]

The skin layer thickness d was unknown for the reflectance calculations, and hence a parametric variation was performed to minimize the mean square error MSE_{ref} as shown in Fig. 12 for several ageing conditions. The final value for d was assumed to be 80 Å for all reflectance calculations. Because this thickness is a fraction of the actual thickness of gold (80 nm), the underlying titanium layer was not considered in the model. Similarly, Hansen et al.[21] reported that a change in reflectance is caused by a change in electron concentration in the first 50 Å of bulk gold.

6 Results: High-Voltage Cycling

An increased-voltage study was completed in order to simulate accelerated ageing. The nominal microsupercapacitor was used subsequent to the previously described study. Increasingly higher voltages were applied to the device circuit: 1.4V, 1.6V, and 1.8V. The voltage pulse length remained at 30 ms, which corresponded to increased scan rates for each voltage level. In this case, the reflectance change signal was only recorded at 16 ms into the voltage pulse because it was greatest in magnitude. As previously, each image was averaged over 2,000 cycles (5 minutes). This

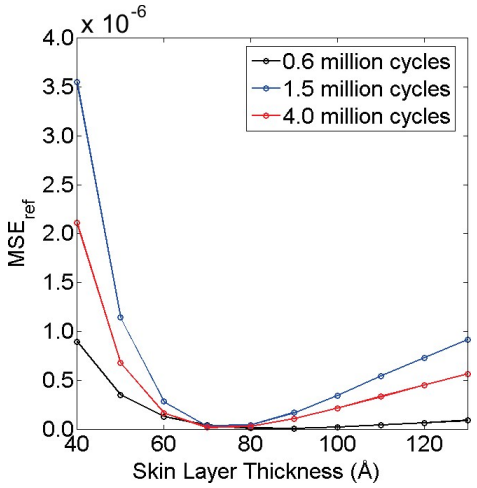

Fig. 12 $(MSE)_{ref}$ as a function of assumed skin layer thickness at various ageing conditions.

modified scheme has the advantage of enabling the record of data points more frequently in terms of number of cycles. On the other hand, the disadvantage is that reflectance change is not recorded at any other time steps during the voltage pulse.

CV curves were recorded between each voltage step, as shown in Fig. 13. The results indicate that the capacitance slightly increased throughout this measurement despite the decreasing trend during the last phase in reflectance measurements. This effect was likely due to the fact that the capacitance was measured at 25 V/s, while the reflectance measurements were recorded at greater scan rates that slightly varied due to the external resistor.

The mean reflectance change and standard deviation results are shown in Fig. 14. The device reflectance did not change significantly during the first phase (1.4V), then began to change during the second phase (1.6V), and clearly degraded during the third phase (1.8V). Because of the presence of the resistor in the circuit, the measured maximum voltages applied to the device were 1.19V, 1.31V, and 1.46V, respectively. We note that PVA electrolyte requires some moisture to function correctly. Electrolysis of water occurs at 1.23V; therefore degradation in performance was expected.

A change in standard deviation of the reflectance images was also observed. During the second phase (1.6V), the standard deviation trend is similar for both electrodes. Therefore, the physical source of this effect was likely the electrolyte. However, a detailed understanding of this trend remains unclear. For the third phase (1.8V), a change in standard deviation occurred only on the negative electrode. The results indicate that the mean did not change significantly, but the reflectance distribution became more varied. This trend was likely related to the visibly-degrading negative electrode in the CCD image. In contrast, the mean for the positive electrode decreased significantly, while the standard deviation remained relatively constant, indicating that the entire electrode was degrading, yet more uniformly.

As shown in Fig. 15, the negative electrode clearly underwent visible ageing during the third phase (1.8V). The effect is consistent with previous references claiming that the negative elec-

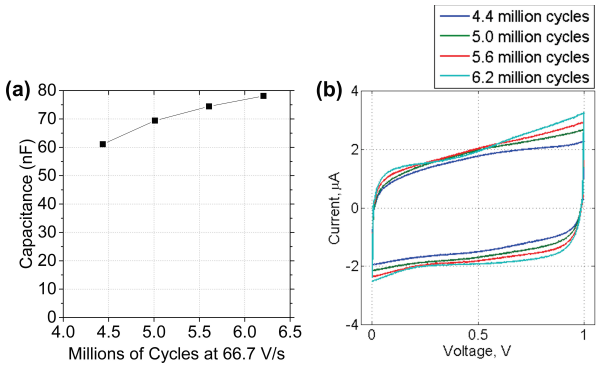

Fig. 13 (a) Capacitance and (b) CV curves of the nominal microsupercapacitor during increased-voltage cycling, all measured at 25 V/s. The applied voltage was increased after each capacitance measurement. Each successive data point refers to capacitance measurements after cycling at v_M=1.0V, 1.4V, 1.6V, and 1.8V.

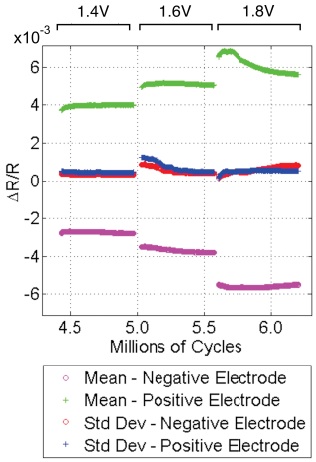

Fig. 14 Mean reflectance change at 16 ms into the voltage pulse during increased voltage cycling. Data were recorded for applied voltages of v_M =1.4V, 1.6V, and 1.8V.

trode is subject to more degradation. However, it seemed that this degradation did not strongly affect the reflectance change. Recall that this electrode primarily interacted with the H^+ ions. Because the degradation was limited to a single electrode, we conclude that the bulk electrolyte was not the cause of the ageing, but rather the electrode surface changed. An edge effect along the outline of each electrode finger is also evident in the CCD image. The degradation is less apparent toward the lead-side of the device (toward the right in the image), as the electric field may be weaker in that area. Further, individual defect spots emerged on the CCD image and became visible on the reflectance image, as highlighted in Fig. 15.

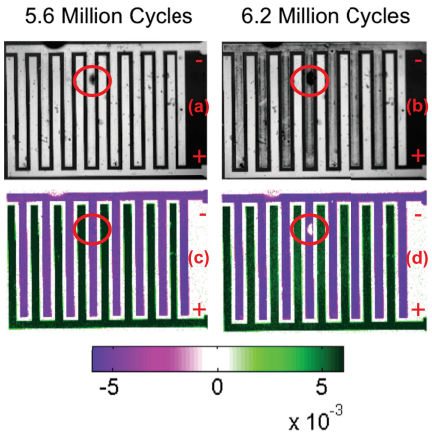

Fig. 15 (a,b) CCD and (c,d) reflectance images (a,c) before and (b,d) after cycling with an applied voltage of 1.8V to the test circuit during the increased-voltage experiment. Annotation highlights individual defect areas.

7 Conclusion

Gold microsupercapacitors with interdigitated electrodes were studied using an electroreflectance method. Reflectance and CCD images were recorded over a period of 4.1 million cycles for a nominal device and a device with initial nonuniform charge behavior. The performance of the nominal device had insignificant changes in reflectance and capacitance. In contrast, the capacitor with burn-in behavior exhibited two phases of ageing behavior. The reflectance images and equivalent circuit model supported the hypothesis that the device behavior was first dominated by wetting of the electrolyte followed by ohmic leakage through the electrolyte. Next, an accelerated ageing test demonstrated that the negative electrode is impacted more greatly in response to increased voltage, as visualized from CCD images. To complete the study, a numerical model included the relationship between electrode charge accumulation and reflectance change and furthermore successfully predicted the observed reflectance signal.

8 Acknowledgements

Financial support for this work provided by the MURI program on Nanofabrication of Tunable 3D Nanotube Architectures (PM: Dr. Joycelyn Harrison, Grant: FA9550-12-1-0037), the National Science Foundation's Scalable Nanomanufacturing program (Grant: CMMI-1344654), and the Indiana Next Generation Manufacturing Competitiveness Center is gratefully acknowledged. Authors are also grateful to the staff members of the Birck Nanotechnology Center at Purdue University for their support and cooperation. The authors acknowledge Guoping Xiong for insight regarding device fabrication and testing. The authors also thank Ritu Gupta for discussion and contributions to sample fabrication.

References

1 R. W. Hart, H. S. White, B. Dunn and D. R. Rolison, *Electrochem. commun.*, 2003, **5**, 120–123.

2 G. Xiong, C. Meng, R. G. Reifenberger, P. P. Irazoqui and T. S. Fisher, *Electroanalysis*, 2014, **26**, 30–51.

3 G. Wang, L. Zhang and J. Zhang, *Chem. Soc. Rev.*, 2012, **41**, 797–828.

4 A. Ponrouch, S. Garbarino, E. Bertin and D. Guay, *J. Power Sources*, 2013, **221**, 228–231.

5 W.-W. Liu, Y.-Q. Feng, X.-B. Yan, J.-T. Chen and Q.-J. Xue, *Adv. Funct. Mater.*, 2013, **23**, 4111–4122.

6 R. Lucio-Porto, S. Bouhtiyya, J. Pierson, a. Morel, F. Capon, P. Boulet and T. Brousse, *Electrochim. Acta*, 2014, **141**, 203–211.

7 Y. G. Zhu, Y. Wang, Y. Shi, J. I. Wong and H. Y. Yang, *Nano Energy*, 2014, **3**, 46–54.

8 W. Gao, N. Singh, L. Song, Z. Liu, A. L. M. Reddy, L. Ci, R. Vajtai, Q. Zhang, B. Wei and P. M. Ajayan, *Nat. Nanotechnol.*, 2011, **6**, 496–500.

9 M. Xue, F. Li, J. Zhu, H. Song, M. Zhang and T. Cao, *Adv. Funct. Mater.*, 2012, **22**, 1284–1290.

10 M. F. El-Kady and R. B. Kaner, *Nat. Commun.*, 2013, **4**, 1475.

11 Y. Lim, J. Yoon, J. Yun, D. Kim, S. Y. Hong, S.-j. Lee, G. Zi and J. S. Ha, *ACS Nano*, 2014, **8**, 11639–11650.

12 E. H. El Brouji, O. Briat, J. M. Vinassa, N. Bertrand and E. Woirgard, *IEEE Trans. Veh. Technol.*, 2009, **58**, 3917–3929.

13 O. Bohlen, J. Kowal and D. U. Sauer, *J. Power Sources*, 2007, **172**, 468–475.

14 G. Xiong, A. Kundu and T. Fisher, *Thermal Effects in Supercapacitors*, Springer International Publishing, 2015.

15 P. Ratajczak, K. Jurewicz, P. Skowron, Q. Abbas and F. Béguin, *Electrochim. Acta*, 2014, **130**, 344–350.

16 X. Lu, T. Liu, T. Zhai, G. Wang, M. Yu, S. Xie, Y. Ling, C. Liang, Y. Tong and Y. Li, *Adv. Energy Mater.*, 2014, **4**, 1–6.

17 D. Cericola, R. Kotz and A. Wokaun, *J. Power Sources*, 2011, **196**, 3114–3118.

18 A. M. Bittner, M. Zhu, Y. Yang, H. F. Waibel, M. Konuma, U. Starke and C. J. Weber, *J. Power Sources*, 2012, **203**, 262–273.

19 J. Feinleib, *Phys. Rev. Lett.*, 1966, **16**, 1200–1202.

20 A. Prostak and W. N. Hansen, *Phys. Rev.*, 1967, **160**, 600.

21 W. N. Hansen and A. Prostak, *J. Phys. Chem. Solids*, 1968, **174**, 500–503.

22 B. Seraphin, *Surf. Sci.*, 1969, **13**, 136–150.

23 J. L. McNatt, *Phys. Rev. Lett.*, 1969, **23**, 915–918.

24 T. Takamura, K. Takamura and E. Yeager, *J. Electroanal. Chem. Interfacial Electrochem.*, 1971, **29**, 279–291.

25 B. E. Conway, *Electrochemical Supercapacitors: Scientific Fundamentals and Technological Applications*, Klewer Academic / Plenum Publishers, New York, 1st edn, 1999.

26 K. Maize, A. Kundu, G. Xiong, K. R. Saviers, T. S. Fisher and A. Shakouri, *Analyst*, 2016, in peer review.

27 N. Omar, F. Van Mulders, J.-M. Timmermans, J. Van Mierlo, P. V. D. Bossche and H. Culcu, EVS24 Int. Batter. Hybrid Fuel Cell Electr. Veh. Symp., 2009, pp. 1–11.

28 A. G. Pandolfo and A. F. Hollenkamp, *J. Power Sources*, 2006, **157**, 11–27.

29 H. A. Andreas, *J. Electrochem. Soc.*, 2015, **162**, A5047–A5053.

30 J. D. D. E. Mcintyre and D. Aspnes, *Surf. Sci.*, 1971, **24**, 417–434.

31 H. Ehrenreich and H. Philipp, *Phys. Rev.*, 1962, **128**, 1622–1629.

32 W. J. Anderson and W. N. Hansen, *Electroanal. Chem. Interfacial Electrochem.*, 1973, **47**, 229–243.